Electronic Supplementary Information

Unsaturated iron ion based coordination polymer for highly efficient photocatalytic hydrogen evolution with simultaneous real wastewater degradation: Mechanistic insight into multifunctional Fe-N sites

Qiuchen Wang[#,a], Jun Ma[#,a], Gen Li[a], Tianxiang Zhao[a], Peng Chen*[,a], Fei Liu*[,a], Shuang-Feng Yin*[,b]

[a] Provincial Guizhou Key Laboratory of Green Chemical and Clean Energy Technology, School of Chemistry and Chemical Engineering, Guizhou University, Guiyang 550025, Guizhou, China

[b] State Key Laboratory of Chemo/Biosensing and Chemometrics, Provincial Hunan Key Laboratory for Cost-effective Utilization of Fossil Fuel Aimed at Reducing Carbon-dioxide Emissions, College of Chemistry and Chemical Engineering, Hunan University, Changsha 410082, Hunan, China

E-mail: pchen3@gzu.edu.cn (P. Chen), jma3@gzu.edu.cn (J. Ma), ce.feiliu@gzu.edu.cn (F. Liu), sf_yin@hnu.edu.cn (S. F. Yin)

These authors contribute equally to this work.

Table S1. The components of organic wastewater before and after reaction from brewing liquor (the information obtained by HPLC-MS (Shiyanjia Lab (www.shiyanjia.com)).

Entry	Organics (before)	Quantitative %	Organics (after)	Quantitative %
1	2-Butanone	10.89	2-Butanone	6.36
2	Ethanol	3.53	Ethanol	1.21
3	2-Butanol, (R)-	22.2	2-Butanol	8.02
4	Acetic acid	11.26	Acetic acid	7.44
5	Propanoic acid	4.29	Propanoic acid	3.66
6	Butanoic acid	7.62	Butanoic acid	5.08
7	2-Furanmethanol	1.91	2-Furanmethanol	0.92
8	Pentanoic acid	1.12	Pentanoic acid	1.06
9	Hexanoic acid	1.98	Hexanoic acid	1.79
10	Phenylethyl Alcohol	5.75	Phenylethyl Alcohol	3.85
11	Phenol, 2,4-bis(1,1-dimethylethyl)-	5.93	Phenol, 2,4-bis(1,1-dimethylethyl)-	5.65
12	Butanoic acid, 3-methyl-	3.81	Benzoic acid	0.14
13	n-Hexadecanoic acid	1.15	Hydrocinnamic acid	0.14
14	(R)-(-)-2-Amino-1-propanol	2.45	Octanoic acid	0.627
15	Octadecanoic acid	0.37	Cyclohexane, 1-ethenyl-3-methylene-5-(1-propenylidene)-	0.36

#	Compound	Value	Compound	Value
16	Squalene	0.29	Benzaldehyde, 3-methyl-	0.04
17	Propane, 1-chloro-2-methyl-	0.81	Formamide	0.23
18	Butyric acid, 2-tridecyl ester	0.07	1-Hexanol, 2-ethyl-	0.04
19	2- Chloropropionic acid, decyl ester	0.02	Propane, 1-nitro-	0.17
21	1-Aminocyclopentane hydroxamic acid	0.03	Urea	0.05
22	3-Cyclohexene-1-carboxylic acid	0.08	1-Propanol	0.11
23	Borazine, 1,3-dimethyl-	0.04	aliphatic hydrocarbons	5.13
24	Benzothiophene, 5-chloro-3-methyl-2-(2-phenyl-4-thiazolyl)-	0.04	aromatic compounds	3.07
25	Pyrazine, trimethyl-	0.05		
26	Sulfurous acid, pentyl tridecyl ester	0.26		
27	Phenol, 2,2'-methylenebis[6-(1,1-dimethylethyl)-4-methyl-	0.43		
28	Dodecane, 2,6,11-trimethyl-	0.15		
29	5H-Thiazolo[3,2-a]pyrimidine-6-carboxylic acid, 5-imino-, ethyl ester	0.01		
30	4-Hexenoic acid, 2-acetyl-2-methyl-, ethyl ester, (E)-	0.02		
31	Pentadecane, 8-hexyl-	0.28		
32	Hexadecane, 2,6,11,15-tetramethyl-	0.09		
33	Tributyl acetylcitrate	0.03		
34	aliphatic hydrocarbons	12.31		
35	aromatic compounds	6.25		

Table S2. Estimation of Fe, C, N and S contents of as-fabricated samples by XPS.

Samples	Fe	C	N	S
TMT	-	47.2	25.4	27.4
FeS	43.4	55.6	-	-
FeTMT	10.6	51.0	19.5	20.9

Table S3. AQY of H_2 evolution and COD value over FeTMT.

Wavelength (nm)	400	420	450	500	550	600
H_2 evolution rate (μmol/h)	11.78	15.92	4.95	2.63	1.01	0.85
Light intensity (mW/cm^2)	9.7	13.3	14.6	16.2	12.2	16.6
Irradiation area (cm^2)	9	9	9	9	9	9
AQY (%)	2.24	2.10	0.55	0.23	0.12	0.06
COD (mg/L)	193.5	220.9	283.7	286.14	308.5	329.8
pH	4.73	5.01	4.57	4.52	3.96	3.95

Table S4. Comparison of different catalysts for photocatalytic HER.

| Entry	Catalyst	Targeted Pollutants	Reaction condition	H_2 generation rate (μmol g^{-1} h^{-1})
S1	Pt/TiO$_2$	Formaldehyde	50 mg of the photocatalyst, 50 mL of an aqueous, UV illumination	1080
S2	Pt−Ti^{18}O$_2$	naphthalene	15 mg of the photocatalyst, 2.44×10^{-4} mol/L of naphthalene solution, $\lambda = 320 \sim 380$ nm	900

S3	Carbon quantum dots/CdS quantum dots /g-C_3N_4	pnitrophenol	50 mg of the photocatalyst, 10 mg/L of organic pollutants solution, $\lambda > 420$ nm	9.4
S4	Cu_2O/RGO /$BiVO_4$	tetracycline	50 mg of the photocatalyst, 30 mL of tetracycline solution, $\lambda > 420$ nm	5.9
S5	S-pCN/$WO_{2.72}$	tetracycline	100 mg of the photocatalyst, 100 mL of TC solution, $\lambda > 420$ nm	786
S6	graphene quantum dots/Mn-N-TiO_2/g-C_3N_4	p-nitrophenol, diethyl phthalate and ciprofloxacin	45 mg of photocatalyst, 80 mL of organic pollutant solution, 3 wt% Pt, $\lambda > 320$ nm	820
S7	C/X-TiO_2@C_3N_4	p-chlorophenol and rhodamineB	100 mg of the photocatalyst, 20 mg/L of organic pollutant solution, 3 wt% Pt, $\lambda > 420$ nm	18.3
S8	Pt(2%)/C_3N_4	p-chlorophenol (PCP), p-nitrophenol (PNP), methylene blue (MB), rhodamine B	100 mg of photocatalyst, 100 ml of 20 mg/L organic pollutant solution, $\lambda > 420$ nm	1.6
S9	2D BP/2D C_3N_4	bisphenol A	20 mg of photocatalyst, 100 mL of 10 mg/L BPA solution, $\lambda > 400$ nm illumination	259.04
S10	Rh-doped $SrTiO_3$	phenol	100 mg of photocatalysts, 2 mmol/L $FeCl_2$ solution, 300W xenon	1.90
S11	Au NPs on sheaf-like TiO_2	ibuprofen	50 mg of photocatalyst, 15 mg/L of ibuprofen solution, 300W xenon	94.5
S12	$ZnIn_2S_4$/$ZnTiO_3$ /$CaIn_2S_4$	Acid Orange II	50 mg of photocatalyst, 500 mL of Acid Orange II aqueous solution, 300W xenon	59.6
S13	g-C_3N_4	tetracycline	50 mg of photocatalyst, 5 mg/L of tetracycline solution, 2 wt% Pt, 300W xenon	325

| S14	CuO/WO$_3$/CdS	methylene blue	5 mg of photocatalyst, 100 mL of 10mg/L MB solution, 300W xenon	44.5
S15	Ag/g-C$_3$N$_4$-Ag-Ag$_3$PO$_4$	levofloxacin	100 mg of the photocatalyst , 10mg/L of LEV aqueous solution, λ > 400 nm	697
This work	☐FeTMT	real wastewater from brewing liquor	20 mg of the photocatalyst, 50 mL of real wastewater from brewing liquor, λ > 420 nm illumination	1272

Fig. S1. Photograph of multi-channel photocatalytic reaction system.
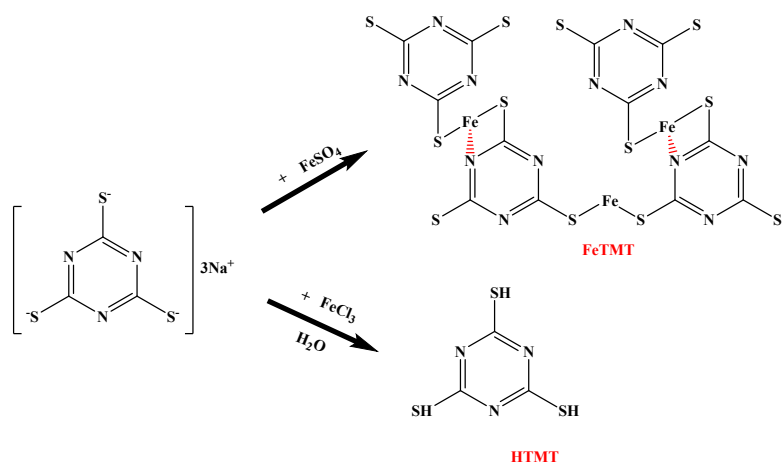
Fig. S2. Schematic of the preparation strategy for FeTMT
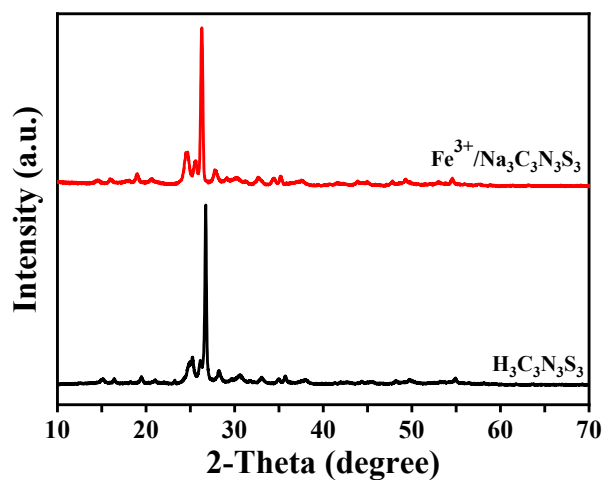
Fig. S3. XRD patterns of as-prepared sample by added Fe^{3+} into the $Na_3C_3N_3S_3$ solution.
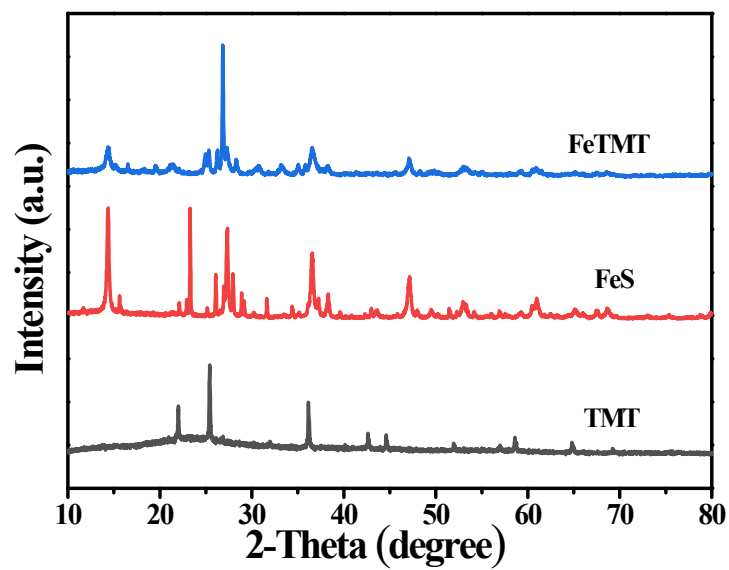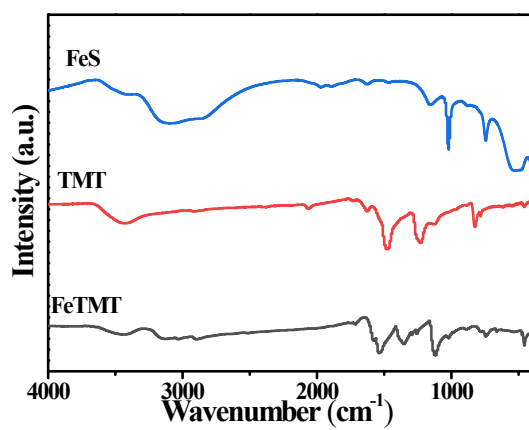
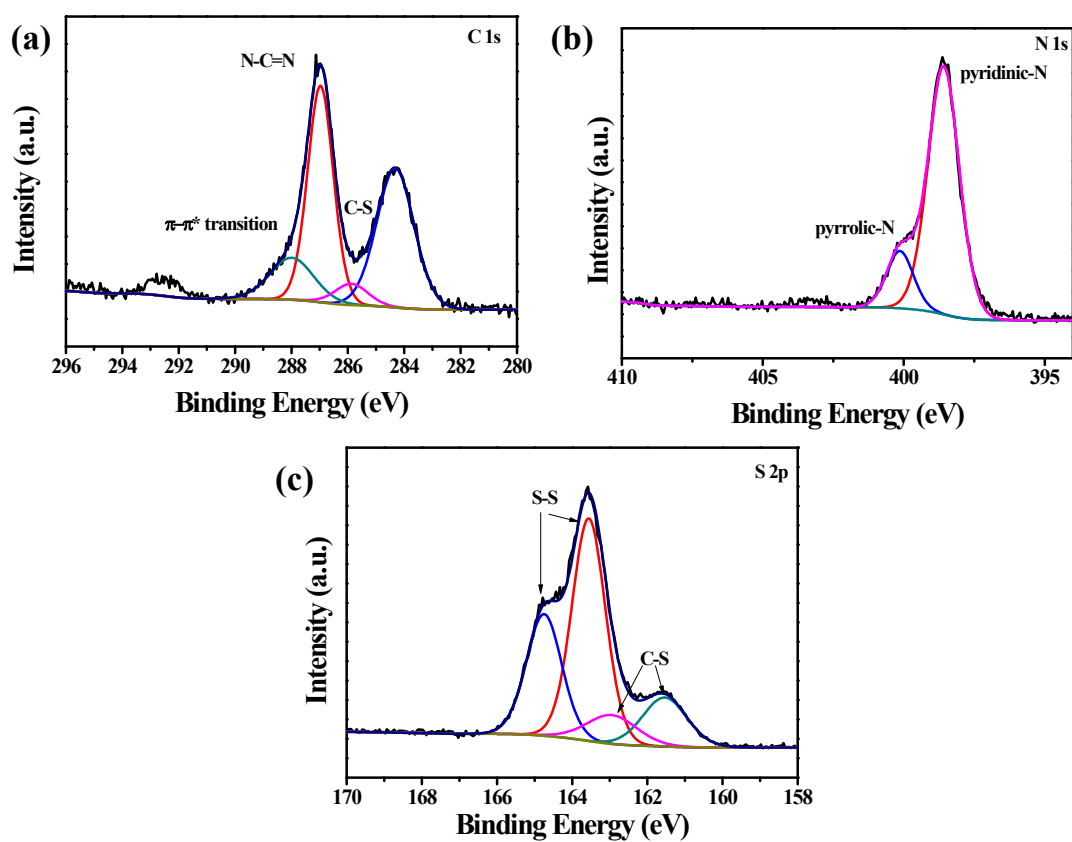**Fig. S4.** XRD patterns of as-prepared samples.
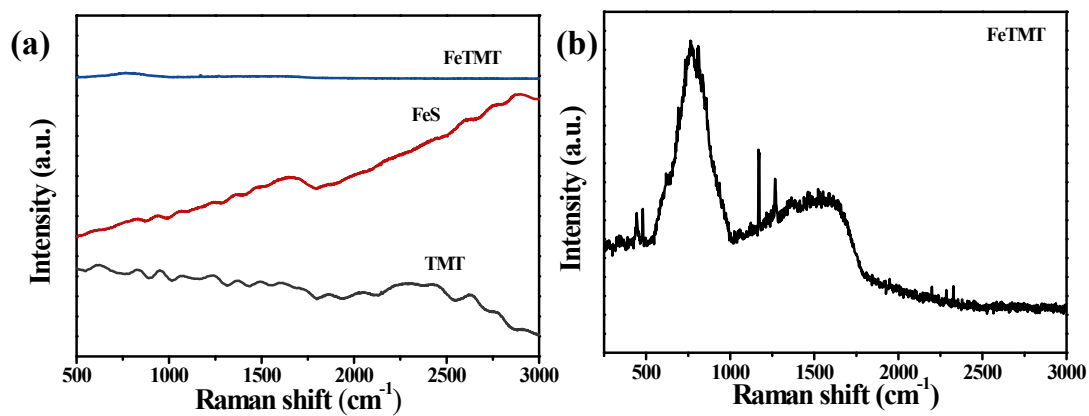
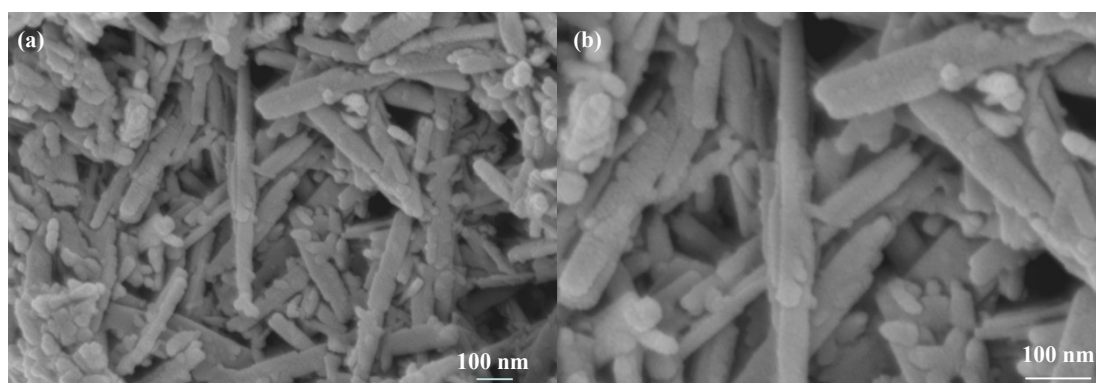**Fig. S5.** Raman spectra of (a) as-prepared samples and (b) FeTMT.

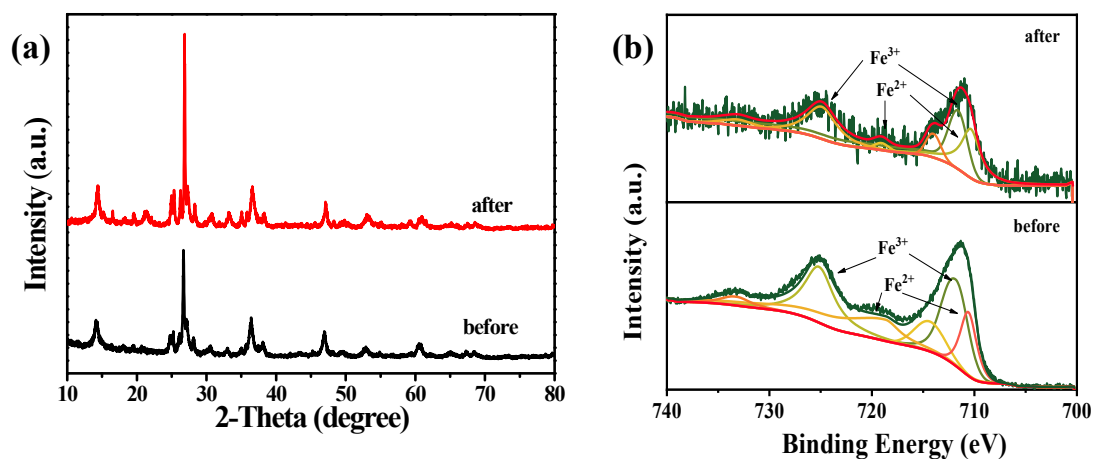**Fig. S6.** FTIR spectrum of as-prepared samples.

Fig. S7. XPS spectra of (a) C1s (b) N 1s (c) S 2p and Fe 2p (B) over $C_3N_3S_3$.


**Fig. S8.** (a-b) SEM images of FeTMT.

Fig. S9. XRD (a) and XPS (b) patterns of FeTMT before and after five cycles of reaction.

From the **Fig. S9a**, there is no apparent change of phase structure, evidencing high recyclability of the as-prepared photocatalyst. As shown in **Fig. S9b**, two main peaks around 710.4 and 718.9 eV represented the Fe (Ⅱ) of 2p3/2 and 2p1/2, respectively. The peak also observed at 712.0 and 724.7 eV could be assigned to Fe^{3+} species, indicating the FeTMT still existed mixed valence of between +2 and +3. Besides, the molar ratio of Fe^{2+}/ Fe^{3+} before and after five cycles of reaction is 0.53 and 0.51 by XPS, respectively, suggesting no change has occurred in the valencestates of Fe ions.
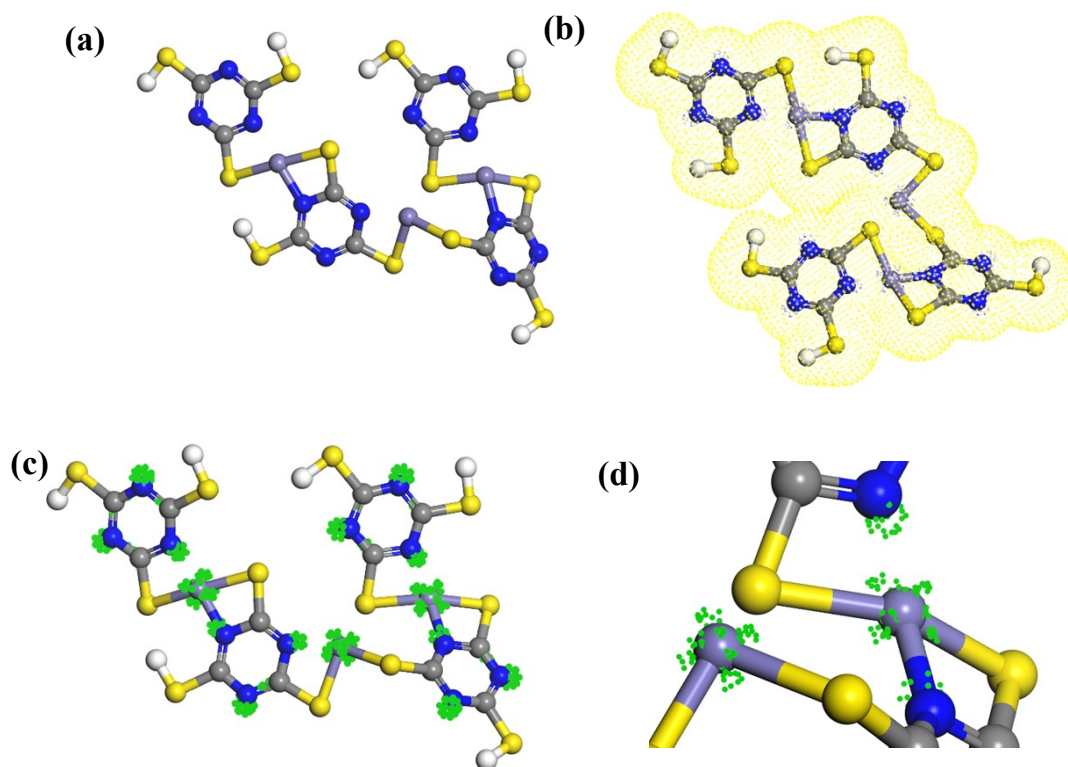
Fig. S10. (a) structure model and (b-d) electron densityof FeTMT (S yellow, N blue, C grey, Fe dark grey, electron green).
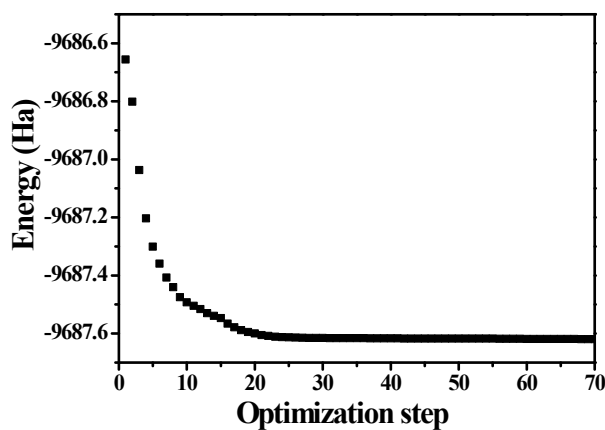

Fig. S11. Optimized structure and energy change curve by materials studio software.

The FeTMT was prepared by a facile wet-chemical method. The typical molecular structure of FeTMT was determined by instrumental characterizations and numerical optimization XPS, XRD and FTIR. The FeTMT structure of geometry optimization by materials studio software was shown in **Fig. S10a**. **Fig. S11** shows

the result of curve of energy changing with steps in geometry optimization. Obviously, the energy of the FeTMT structure tend to be stable in 70 steps. Under this equilibrium status, the structure reaches the lowest energy, which can be further applied to the following density function theory (DFT) calculation.

The Dmol3 module in the materials studio (MS) software was used to investigate the density of states (DOS), electron density (ED) and density field of FeTMT. Calculation accuracy was chosen ultra-fine. BLYP exchange correlation function in generalized gradient approximation (GGA) was selected. All electron nuclear treatment mode and pseudo potential double numerical polarization basis set (DNP) were selected for the calculation.[S16] The convergence criterion of self consistent field was 1×10^{-5} Ha. The convergence criterion of SCF was 1×10^{-6} Ha. The convergence criterion of DFT calculation was 0.004 ha/Å. After the simulation, the analysis module of MS was used to analyze the results
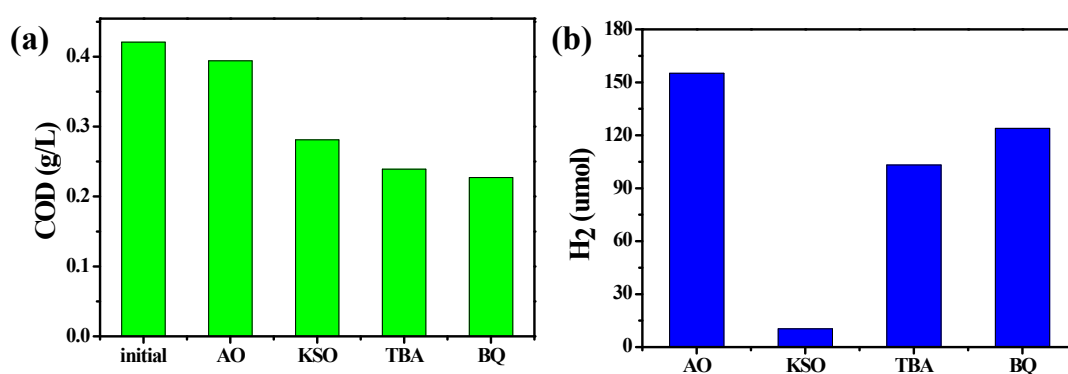
Fig. S12. Photocatalytic degradation of (a) real wastewater and (b) H_2 production over FeTMT with or without a scavenger. Ammonium oxalate (AO), Potassium persulfate (KSO), p-benzoquinone (BQ) and tert-butanol (TBA) as scavengers for hole (h^+),

electron (e^-), superoxide radical ($O_2^{\cdot-}$) and hydroxyl radical ($\cdot OH$) trapping, respectively.
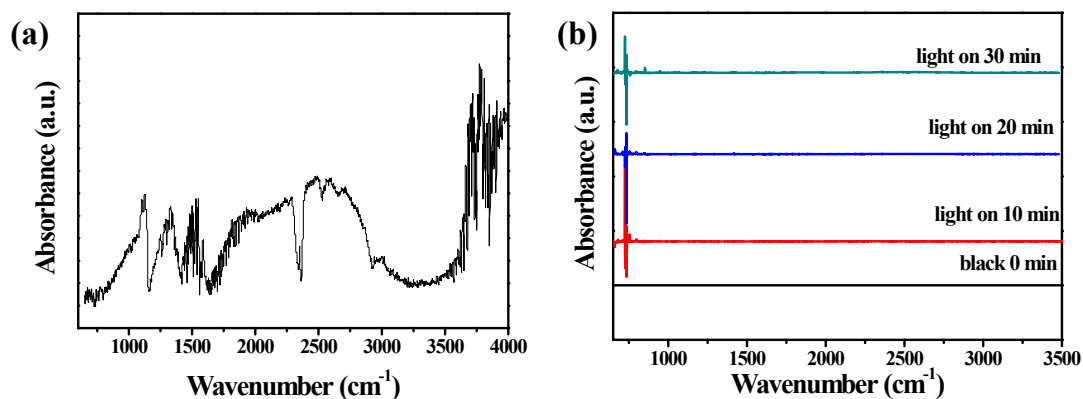
Fig. S13. *In situ* infrared spectroscopic experiments of (a) before and (b) after illumination over FeTMT.

The in situ FT-IR measurements were tested by a Shimadzu IR Affinity-1 spectrometer equipped with a customized chamber. Typically, the chamber was filled with liquid nitrogen, and the FTMT get wet with waste water. Prior to light irradiation, the reaction system was filled with nitrogen. The in situ infrared spectral data were recorded by IR software at certain intervals.

Fig. S14. Real wastwater contact angle of the FeTMT (26.2°), FeS (36.0°), TMT (42.6°).

References

[S1] H. Belhadj, S. Hamid, P. K. J. Robertson and D. W. Bahnemann, *ACS Catal.*, 2017, **7**, 4753−4758.

[S2] S. Kampour and K. C. Stylianou, *ACS Catal.*, 2019, **9**, 4247.

[S3] X.-H. Jiang and L.-C. Wang, F. Yu, Y.-C. Nie, Q.-J. Xing, X. Liu, Y. Pei, J.-P. Zouand W.-L. Dai, *ACS Sustain. Chem. Eng.*, 2018, **6**, 1269.

[S4] H. Shen, M. Wang, X. Zhang, D. Li, G. Liu and W. Shi, *Fuel*, 2020, **280**, 118618.

[S5] X. Li, B. Kang, F. Dong, Z. Zhang, X. Luo, L. Han, J. Huang, Z. Feng, Z. Chen, J. Xu, B. Peng and Z. L. Wang, *Nano Energy*, 2021, **81**, 105671.

[S6] Y.-C. Nie, F. Yu, L.-C. Wang, Q.-J. Xing, X. Liu, Y. Pei, J.-P. Zou, W.-L. Dai, Y. Li and S.-L. Suib, *Appl. Catal. B Environ.*, 2018, **227**, 312.

[S7] K. Li, Z. Zeng, L. Yan, M. Huo, Y. Guo, S. Lu and X. Luo, *Appl. Catal. B Environ.*, 2016, **187**, 269.

[S8] K. Li, Z. Zeng, L. Yan, S. Luo, X. Luo, M. Huo and Y. Guo, *Appl. Catal. B. Environ.*, 2015, **165**, 428.

[S9] X. Zhang, J. Deng, J. Yan, Y. Song, Z. Mo, J. Qian, X. Wu, S. Yuan, H. Li and H. Xu, *Appl. Surf. Sci.*, 2019, **490**, 117.

[S10] D. Li, J. C.-C. Yu, V.-H. Nguyen, J. C. S. Wu and X. Wang, *Appl. Catal. B Environ.*, 2018, **239**, 268.

[S11] X. Yao, X. Hu, Y. Liu, X. Wang, X. Hong, X. Chen, S. C. Pillai, D. D. Dionysiou and D. Wang, *Chemosphere*, 2020, **261**, 127759.

[S12] J. Wang, D. Wang, X. Zhang, C. Zhao, M. Zhang, Z. Zhang, J. Wang, *Int. J. Hydrog. Energy*, 2019, **44**, 6592.

[S13] Z. Chen, S. Li, Y. Peng and C. Hu, *Catal. Sci. Technol.*, 2020, **10**, 5470.

[S14] D. Wang, J. Liu, M. Zhang, Y. Song, Z. Zhang and J. Wang, *Appl. Surf. Sci.*, 2019, **498**, 143843.

[S15] S. Li, M. Zhang, Z. Qu, X. Cui, Z. Liu, C. Piao, S. Li, J. Wang and Y. Song, *Chem. Eng. J.*, 2020, **382**, 122394.

[S16] S. Grimme, J. Antony, S. Ehrlich, H. Krieg, *J. Chem. Phy.,* 2010, **132**, 154104.